Interdependence of the electrical and optical properties of liquid crystals for phase modulation applications

I. R. Guralnik
Department of Physics, Samara State University, 443011, Academican Pavlov Str., 1 Samara, Russia

V. N. Belopukhov
JSC, South-West Oil Product Transport, 443010, Lev Tolsoj Str., 75 Samara, Russia

G. D. Love and A. F. Naumov[a)]
Department of Physics and School of Engineering, University of Durham, South Road, Durham DH1 3LE, United Kingdom

(Received 4 October 1999; accepted for publication 25 January 2000)

The electrical capacitance and conductance of nematic liquid crystal (LC) cells were measured in combination with their optical properties as functions of applied voltage magnitude and frequency. A single experimental system was used in order to determine the correlation between these characteristics. These parameters are crucial for understanding and optimizing the performance of modal LC devices. Both ordinary and dual frequency LCs were investigated. For the latter type, Cole-Cole diagrams show a Debye type frequency dispersion in a limited range of 4–9 kHz. Also, a phenomenological theory of the measured parameters was developed and is in good agreement with experimental data. Two examples are discussed, and they illustrate the importance of taking into account the equivalent conductance of LC cells. © *2000 American Institute of Physics.* [S0021-8979(00)03409-5]

INTRODUCTION

The application of liquid crystal (LC) modulators as phase modulators for real time wave front control is important for the development of inexpensive adaptive optics systems.[1–3] Usually LCs are homogeneously aligned for phase-only modulation. A given distribution of the refractive index, and hence the phase, is defined by the electric field distribution across the aperture. The electric field distribution, in its turn, is produced either by a set of individual electrodes (pixels),[4] by the distribution of light intensity in a photoconductor,[5] or by the field distribution in a modal wave front corrector.[6] The modal control principle facilitates a relatively simple design of cylindrical and spherical adaptive lenses,[7,8] a key element in many optical applications. The use of modal LC modulators and dual frequency control[9,10] in order to improve the LC response time both require a full description of the electrical parameters of the LC, such as the cell capacitance, conductivity and dielectric constants. These are all functions of the applied electric field. In this article we present a model of the LC electrical properties and relate it to experimental results. The main results of this article are (1) to show the qualitative and quantitative connections between the electrical and optical properties of nematic LCs, (2) to demonstrate how these relationships are useful in explaining some of the properties of real LC phase modulators, and (3) to allow advanced control of dual frequency modal LC devices. We begin by outlining the principle of modal LC control to produce lenses. Then we describe the theory of the cell capacitance, conductance, and electrooptical response. Next we compare these with experimental results and draw some conclusions.

A modal liquid crystal corrector (MLCC) can be treated as a system with a distributed electrical resistance of the control electrode and distributed impedance of the LC layer. The applied voltage distribution $V(x,y)$ (x and y are the coordinates along the LC layer) is described by the lens equation:[7]

$$\nabla_S^2 V = \rho_S c \frac{\partial V}{\partial t} + \rho_S g V, \tag{1}$$

where ρ_S is the control electrode sheet resistance, and c and g are the specific capacitance and conductance of the LC layer, respectively. Both c and g are functions of the applied voltage.

For pure-nematic LCs, the dielectric relaxation and the capacitance and conductance have usually been investigated by way of small-signal techniques[11,12] with ac voltages of about 1V. The electric properties have mostly been explored separately from phase delay measurements. Only recently attempts were made[13,14] to relate the retardance $\Delta\Phi$, the ac voltage, and the cell capacitance C. However, in these experiments the equivalent conductivity of the LC cell was not taken into account.

PHENOMENOLOGICAL RELATIONS

Phase-only modulation (with no polarization or intensity modulation) is achieved by the electrooptic S effect in cells based on nematic LCs with an initially planar alignment. In this study we are concerned only with cells of this type. In

a)Electronic mail: a.f.naumov@durham.ac.uk

pure nematic LCs (where there are no free charge carriers) the total current density is represented by the displacement current only:

$$j_i = \frac{\partial D_i}{\partial t}, \quad i = x, y, z, \tag{2}$$

where z is the coordinate normal to the LC layer. When the electric field **E** is directed along z axis, the electric displacement is given by $D_z = \varepsilon_0 \varepsilon E_z$, with $\varepsilon_0 = 8.854 \times 10^{-12}$ F/m and

$$\varepsilon = \varepsilon_\perp \cos^2\theta + \varepsilon_\parallel \sin^2\theta, \tag{3}$$

where $\varepsilon_\perp$ and $\varepsilon_\parallel$ are the perpendicular and parallel components of the dielectric tensor, and θ is the angle of the director.

In Eq. (3) $\varepsilon_\perp$ and $\varepsilon_\parallel$ depend on the frequency of the applied voltage (dispersion of the dielectric constants), but not on its amplitude. It is known from experiment[11] the frequency dispersion of $\varepsilon_\perp$ and $\varepsilon_\parallel$ is manifested in different frequency ranges. The high-frequency dispersion of $\varepsilon_\perp$ corresponds approximately to the Debye relaxation time of an isotropic liquid. That means that $\varepsilon_\perp$ must be mainly contributed to by the rotation of the LC molecules around their long axes, since this rotation is independent of the nematic interaction. The low-frequency dispersion of $\varepsilon_\parallel$ is inherent to the LC state only. Therefore, it must be produced by the rotation of the LC molecules around their short axes. The intermolecular forces that are responsible for the nematic order hamper this rotation, thereby increasing the relaxation time and bringing the dispersion range down to radio frequencies.

Conversely, the angle θ in Eq. (3) is approximately independent of the voltage frequency (within a restricted frequency range), but is a function of its root mean square (rms) value because for practically interesting frequencies of the applied voltage the director cannot follow the instantaneous time variation of the local electric field.

Following these obvious but necessary notes, we can correctly define and calculate the equivalent capacitance and conductance of the LC layer. From Eqs. (2), j_z can be rewritten, using D_z, and $E_z \propto \exp(-i\omega t)$, as

$$j_z = -i\omega\varepsilon\varepsilon_0 E_z. \tag{4}$$

Integrating across the cell thickness we obtain

$$V = \int_{-d/2}^{d/2} E dz = \frac{iI}{\omega C_0}\frac{1}{d}\int_{-d/2}^{d/2}\frac{dz}{\varepsilon(z)} = \frac{iI\langle\varepsilon^{-1}\rangle}{\omega C_0}, \tag{5}$$

where $I = j_z S$ is the total current amplitude, $C_0 = \varepsilon_0 S/d$ is the so called geometric capacitance of the cell, and S and d are the electrodes area and the LC thickness, respectively. The brackets denote averaging over the LC layer thickness.

From Eq. (5) the equivalent G and C parameters can be described in terms of the real and imaginary parts of the LC layer complex dielectric constant:

$$Z^{-1} = \frac{I}{V} = G - i\omega C = \frac{-i\omega C_0}{\langle\varepsilon^{-1}\rangle}, \tag{6}$$

where $C = cS$ and $G = gS$ are the cell's equivalent capacitance and conductance, respectively. Separation of the real and imaginary parts in Eq. (6) yields

$$G = \varepsilon_0 \omega S \cdot \frac{\beta}{\alpha^2 + \beta^2}, \quad C = \varepsilon_0 S \cdot \frac{\alpha}{\alpha^2 + \beta^2}, \tag{7}$$

where we denoted

$$\alpha = \int_{-d/2}^{d/2} \frac{\varepsilon' dz}{\varepsilon'^2 + \varepsilon''^2}, \quad \beta = \int_{-d/2}^{d/2} \frac{\varepsilon'' dz}{\varepsilon'^2 + \varepsilon''^2}, \tag{8}$$

and ε' and ε'' are the real and imaginary parts of the dielectric constant. To calculate the integrals in Eq. (8), the angle θ vs z dependence must be found from the steady-state Ericksen-Leslie's equation of general theory of the S effect (see, for example, Ref. 15) which is given by

$$\frac{\partial}{\partial z}\left[(K_{11}\cos^2\theta + K_{33}\sin^2\theta)\frac{\partial\theta}{\partial z}\right] - (K_{33} - K_{11}) \times \sin\theta\cos\theta\left(\frac{\partial\theta}{\partial z}\right)^2 + \varepsilon_0 \Delta\varepsilon E^2 \sin\theta\cos\theta = 0, \tag{9}$$

where K_{11} and K_{33} represent the splay and bend Frank elastic constants, and

$$E(z) = D_z/\varepsilon_0(\varepsilon_\parallel \sin^2\theta + \varepsilon_\perp \cos^2\theta) \tag{10}$$

is the rms of the applied electrical field.

In the general case, the solution is available only in numerical form. However, for small and large voltages, respectively, the formulas for G and C are straightforward. At voltages below the threshold for the S effect, $V < V_{th}$, the LC director is not realigned, hence $\varepsilon = \varepsilon_\perp$. Otherwise, for $V \gg V_{th}$ the director is everywhere along the field lines except for the narrow regions near the cell walls, giving $\varepsilon = \varepsilon_\parallel$. Then we obtain, from Eqs. (7),

$$G = \omega C_0 \varepsilon''_\gamma, \quad C = \varepsilon'_\gamma C_0, \quad \gamma = \begin{cases} \perp, & \text{for } V < V_{th} \\ \parallel, & \text{for } V \gg V_{th} \end{cases}. \tag{11}$$

The LC retardance, $\Delta\Phi$, is also determined by the orientation of the LC molecules,

$$\Delta\Phi = \frac{2\pi}{\lambda}\int_{-d/2}^{d/2}\left\{\frac{n_\perp n_\parallel}{[n_\perp^2\cos^2\theta(z) + n_\parallel^2\sin^2\theta(z)]^{1/2}} - n_\perp\right\}dz, \tag{12}$$

where $n_\parallel$ and $n_\perp$ are the refractive indices measured along and normal to the optical axis.

Eqs. (7), (11) and (12) provide a basis for the interpretation of the experimental results below, as well as the means for relating the observable G, C, and $\Delta\Phi$ with ε' and ε''.

EXPERIMENTAL RESULTS AND DISCUSSION

We examined the following nematic LCs: LC1348 and LC1001 (NIOPIC, Russia) and E49 (Merck, Germany). We selected these because (1) LC1348 is a typical material used in optically addressed modulators, (2) LC1001 exhibits low-frequency inversion of the dielectric anisotropy, and is useful for high temporal bandwidth applications via dual frequency

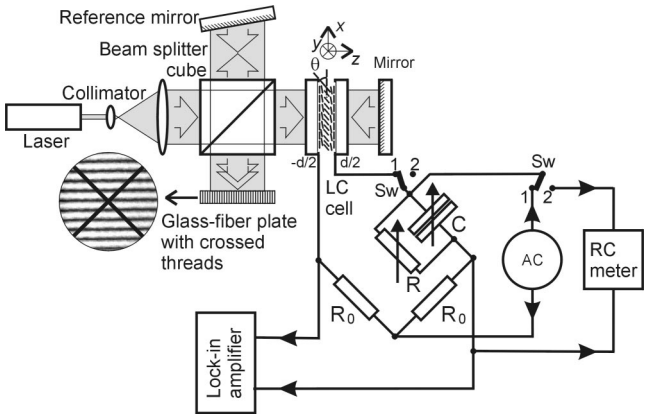

FIG. 1. Experimental setup.

control, and (3) E49 is the most suitable material for fabricating modal wave front correctors due to its high birefringence and low conductivity.

Each LC cell was initially planar aligned, set by a polyvinyl alcohol (PVA) layer deposited onto the transparent electrodes in a centrifuge followed by rubbing of the PVA layer with fabric in one direction. The thickness of the LC layer was set by calibrated polivinyl spacers. The geometry of the cells was as follows: $S=8\ \mathrm{cm}^2$, $d=25\ \mu\mathrm{m}$ for the LC1348 and $S=10\ \mathrm{cm}^2$, $d=5\ \mu\mathrm{m}$ for the LC1001 cells.

The experimental setup is shown in Fig. 1. We used an ac bridge circuit to measure the G and C parameters, with the LC cell in one arm of the bridge and an adjustable capacitor and resistor connected parallel in the other. A sinusoidal generator was connected across one of the bridge diagonals and a lock-in amplifier tuned to the generator frequency across the other. It was necessary to use the lock-in amplifier in order to select only the driving frequency; other frequencies were also generated due to the nonlinear behavior of the LC. With the double switch Sw in position 1 the LC cell was supplied with ac voltage which induces the LC director to reorient by an angle θ, which in turn, varies the effective birefringence and electric characteristics of the cell. By varying the balancing resistance and capacitance of the bridge we minimized the lock-in voltage. Then switch Sw was set into position 2 and the digital RC meter displayed the equivalent capacitance and resistance.

To measure the phase delay, we assembled a Michelson interferometer with the LC cell under investigation in the object arm. The initial alignment of the LC layer coincided with the linear polarization direction of the 0.633 μm He–Ne laser beam. The interference fringe displacement was monitored visually on a glass-fiber plate with a crosshair.

The $C-V$ characteristics at different frequencies $f=\omega/2\pi$ are plotted in Fig. 2. It can be seen that, as the voltage crosses the threshold, the capacitance increases. This is to be expected considering Eqs. (7) and the positive anisotropy ($\varepsilon_\parallel'>\varepsilon_\perp'$) of the LCs. The high-voltage behavior of the capacitance in Fig. 2(c) corresponds to the low-frequency dispersion of ε' for LC1001. With increasing frequency ε' decreases and equals $\varepsilon_\perp'$ at approximately 7 kHz. At higher frequencies the capacitance remains equal to its pre-threshold magnitude over the entire voltage range since the S

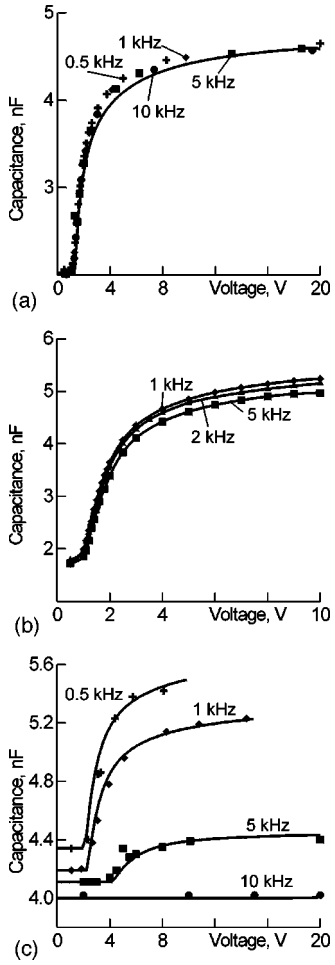

FIG. 2. Alternating Current voltage dependence of the cell capacitance at different frequencies for (a) LC1348, (b) E49 and (c) LC1001. The numbers in the plots denote frequency values.

effect vanishes at zero anisotropy. Figure 3 shows the equivalent conductance, G, as a function of applied voltage. The plots demonstrate that conductance, like capacitance, is determined by the LC molecular realignment. Note the difference in scales indicating the higher conductance of the dispersive LC.

The solid lines in Figs. 2 and 3 represent the theoretical curves calculated using Eqs. (7) and (12) together with steady-state Ericksen–Leslie's equation (9), and the points indicate experimental results. We used the following algorithm for the theoretical approximations. First for each frequency we found the dielectric constants $\varepsilon_\perp'$ and $\varepsilon_\perp''$ by substituting experimental pre-threshold values of G and C into Eqs. (11), respectively. The dielectric constants $\varepsilon_\parallel'$ and $\varepsilon_\parallel''$ were found similarly but using the values of G and C at large voltages. Then we calculated the elastic constant K_{11} from the threshold voltage formula,[11]

$$U_{\mathrm{th}}=\pi\sqrt{\frac{4\pi K_{11}}{\Delta\varepsilon'}}. \tag{13}$$

Next we solved the steady-state Ericksen-Leslie equation for the distribution of the director deformation angle $\theta(z)$ with the voltage as a parameter, and with this distribution the

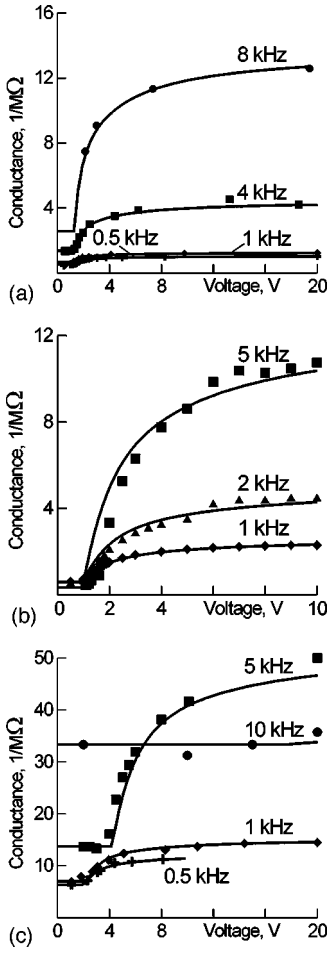

FIG. 3. Alternating Current voltage dependence of the cell conductance at different frequencies for (a) LC1348, (b) E49 and (c) LC1001.

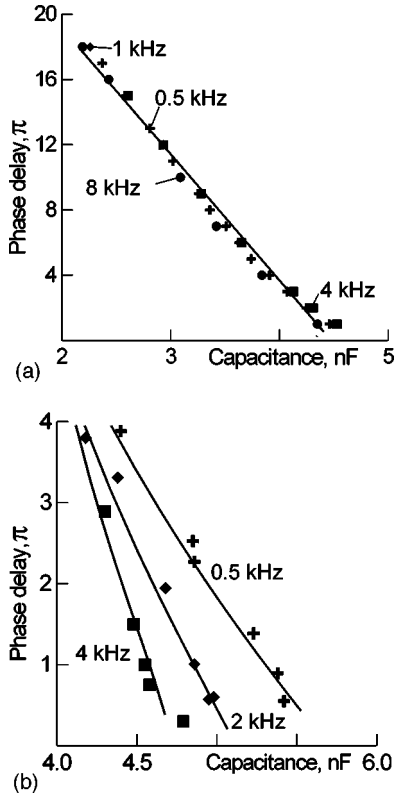

FIG. 4. Phase delay $\Delta\Phi$ vs cell capacitance at different frequencies for (a) LC1348 and (b) LC1001.

integrals in Eq. (8) were calculated according to Eqs. (7) yielding theoretical plots of $C(V)$ and $G(V)$.

To show that both the electrical and optical properties of the LC cells are influenced by the alignment effects, we plotted the electrooptic response vs capacitance and obtained the close to linear curves presented in Fig. 4. This method was recently suggested to linearize the electrooptic response.[13] We see, however, that one should be careful in avoiding dispersion in the frequency range of the LC studied. The electric quality factor of the LC cells, $Q=\omega C/G$, is readily obtained from the plots in Figs. 2 and 3. As expected, $Q \gg 1$ for the nondispersive LC1348 and E49 but $Q \leqslant 1$ for the dispersive LC1001. On the other hand, as we have mentioned earlier, it is the low frequency dispersion that is used for speeding up LC modulators through dual frequency control techniques. Low values of electric quality for such cells indicate that the leakage current can constitute a considerable part of the total current and must be taken into account in designing the driving voltage circuits.

It is instructive to consider the so called Cole-Cole diagram[12] for the LC1001 cell which is plotted in Fig. 5 for $V=10\,\mathrm{V}$ and features the dispersion of $\varepsilon_{\parallel}$. The portion of the plot that can be fitted with a semi-circle corresponds to Debye relaxation. In addition to this, a relatively strong tail of low frequency losses can be seen. This can be explained by the energy dissipation accompanying the frequency realignment of the LC director at low applied frequencies when the LC molecules are capable of following its instantaneous values.

INFLUENCE OF THE DIELECTRIC LOSSES ON THE NEMATIC LC CORRECTORS' PERFORMANCE

Now we want to present two examples illustrating the importance of taking into account the equivalent resistance of the LC layer.

First, we address the problem of dual frequency control of nematic LC cells[10] using LC1001. When we apply a low-frequency electric field (below the crossover frequency that is equal to 7 kHz in our case), the dielectric anisotropy is positive and the LC molecules align along this field. With a

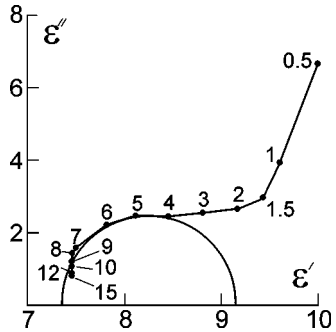

FIG. 5. Cole-Cole diagram for LC1001. The numbers beside the labels are ac voltage frequencies.

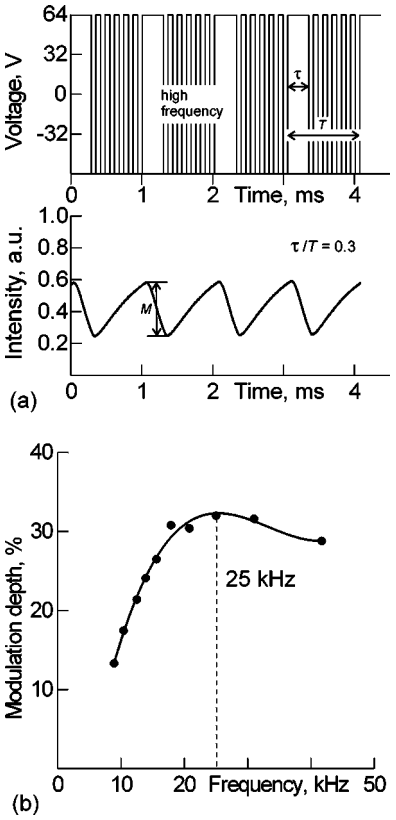

FIG. 6. Influence of the high-frequency component on the modulation depth: (a) shape of the control voltage (top) and electrooptical response (bottom); (b) dependency of the modulation depth vs the high-frequency value.

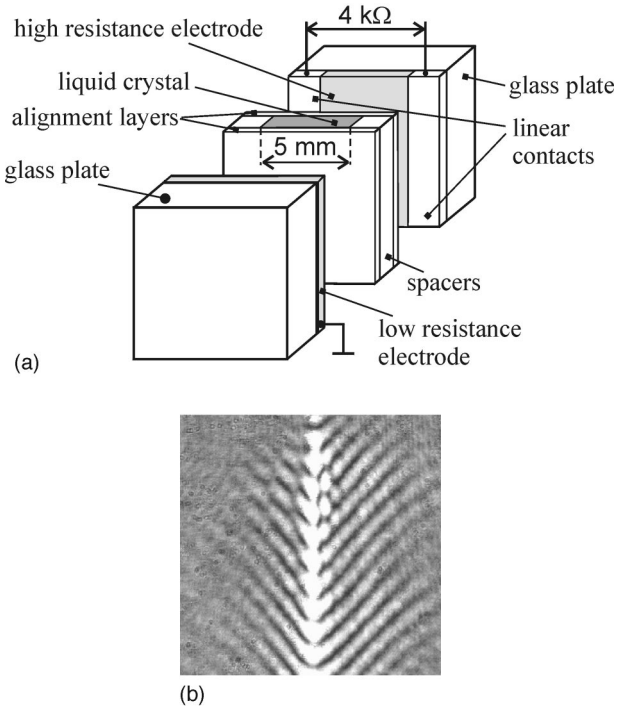

FIG. 7. (a) Schematic design of a MLCC with linear equidistant electrodes and (b) interferogram for frequency corresponding to dielectric constant dispersion: $f=870$ kHz, $V=4$ V.

high-frequency electric field applied, the LC molecules align normally to the field. The modulus of the dielectric anisotropy defines the efficiency of the LC molecular alignment by the applied electric field: larger values of $\Delta\varepsilon'$ cause a faster response. For frequencies above the crossover frequency the dielectric anisotropy is negative and with increasing frequency its modulus also increases. This should produce faster alignment of the molecules for higher frequencies. To check this, we placed the LC cell between crossed polarizers with its initial alignment 45° to the axes of the polarizers. We fixed the amplitude at ± 64 V and the duration ratio between low- and high-frequency voltages at 0.3 with a total period of 1 ms [see Fig. 6(a)]. Then we changed the value of only the high frequency. The resulting ratio, M, of the mean modulation amplitude of laser beam intensity to the maximum modulation depth, when the phase delay varies from 0 to π, is shown in Fig. 6(b). This dependency should show a montonic increase because the modulus of $\Delta\varepsilon'$ increases at $f>f_c$ and reaches saturation at $5-7f_c$. However, experimentally we found the existance of the optimal value of the applied high frequency at which M is maximal. This can be explained by the trade-off between the dielectric losses $\varepsilon''_{\parallel}$ and the dielectric anisotropy $\Delta\varepsilon'$, because the value of the dielectric losses characterized by conductance G in Eq. (11) is growing with frequency and has not saturated. Thus the optimal frequency should exist, and should correspond to the equilibrium between the alignment energy and the energy of the dielectric losses. In this experiment, the optimal frequency is equal to 25 kHz for a square-wave control voltage.

Second, the amplitude-frequency control of a MLCC usually results from a variation of the effective reactance of the system. For low sheet resistance values when the control voltage frequency and the integral resistance of the control electrode R satisfy the condition $f<(RC)^{-1}$, the distribution of the control voltage modulus over the aperture should essentially be uniform. For example, for the LC cell shown in Fig. 7(a) with a resistance between equidistant linear contacts $R=4$ kΩ and average capacitance 0.4 nF the value $(RC)^{-1}$ is equal to 1.6 MHz. However at frequencies of 850–900 kHz we still observed phase inhomogeneities. Figure 7(b) shows the interference pattern for a rms of 4 V and $f=870$ kHz. The picture was obtained using the Michelson interferometer adjusted to give initially straight fringes perpendicular to the LC contacts. Therefore, the phase distribution variation across an aperture corresponds to the deformation of the fringes. The experimental setup is shown in Fig. 1. The reduction in picture contrast in Fig. 7(b) is explained by the dynamic scattering at the periphery of the MLCC aperture that results from the high conductance of the LC at high frequencies.

To explain such behavior, we note that due to the dispersion of the dielectric constants, at certain frequencies its imaginary part ε'' displays resonance behavior. At such frequencies the LC layer conductance g may increase enough to cause lateral gradients of applied voltage in the control electrode of the MLCC. We believe this sudden rise in g to be responsible for focusing by the MLCC based on the relatively low resistance control electrode. To prove the active nature of the LC impedance in this frequency range, we measured the phase shift between the throughput current of the

lens and the applied voltage with a digital phase meter and obtained values of about 11°. Thus, the LC layer capacitance is effectively shunted by its conductance due to the leakage currents in the LC.

CONCLUSION

In this work we experimentally investigated electrical and optical parameters of cells with different LC materials. Phenomenological formulas that we subsequently used for the numerical simulations of adaptive spherical and cylindrical lenses were derived. Comparison of the optical and electrical characteristics of the LC with the low-frequency inversion of the dielectric anisotropy enabled us to elicit specific features of the realignment of its molecules. By analyzing the voltage and frequency dependencies of the electric parameters of the LC, the existence of an optimal value of the high-frequency voltage in dual-frequency control was explained, as was the nonuniformity of the phase distribution over the aperture in a MLCC at high control voltage frequencies.

ACKNOWLEDGMENTS

The authors are deeply grateful to M. Loktev for providing the software for simulating the electrooptic parameters of the nematic LC cells. Two of the authors (A.F.N. and V.N.B.) also thank the European Office of Aerospace Research and Development, which initiated these investigations.

[1] S. R. Restaino, D. Payne, M. Anderson, J. T. Baker, S. Serati, and G. C. Loos, Proc. SPIE **3353**, 775 (1998).
[2] J. Gourlay, G. D. Love, P. M. Birch, and R. M. Sharples, Opt. Commun. **137**, 17 (1997).
[3] M. A. Vorontsov, V. A. Katulin, and A. F. Naumov, Opt. Commun. **71**, 35 (1989).
[4] G. D. Love, Appl. Opt. **36**, 1517 (1997).
[5] A. A. Vasilev, M. A. Vorontsov, A. V. Koryabin, A. F. Naumov, and V. I. Shmalgauzen, Kvant. Elektron. (Moscow) **16**, 599 (1989)
[6] A. F. Naumov and G. V. Vdovin, Opt. Lett. **23**, 1550 (1998).
[7] A. F. Naumov, M. Yu. Loktev, I. R. Guralnik, and G. Vdovin, Opt. Lett. **23**, 992 (1998).
[8] A. F. Naumov, M. Yu. Loktev, I. R. Guralnik, and G. V. Vdovin, Proc. SPIE **3684**, 18 (1998).
[9] V. A. Dorezyuk, A. F. Naumov, and V. I. Shmal'gauzen, Sov. J. Tech. Phys. **34**, 1389 (1989).
[10] A. F. Naumov and V. N. Belopukhov, Proc. SPIE **3688**, 476 (1999).
[11] L. M. Blinov, *Electro-Optical and Magneto-Optical Properties of Liquid Crystals* (Wiley, New York, 1983).
[12] W. H. de Jeu, *Physical Properties of Liquid Crystalline Materials* (Gordon and Breach Science, New York, 1980).
[13] K. Hirabayashi, Opt. Lett. **21**, 1484 (1996).
[14] S. Esposito, G. Brusa, and D. Bonaccini, Proceedings of the ICO-16 Conference on Active and Adaptive Optics, Proc. of ICO-16 Conference on Active and Adaptive Optics, Budapest, Hungary, ESO Conference and Workshop Proc. **48**, 289 (1993).
[15] S. T. Wu and C.-S. Wu, Appl. Phys. Lett. **53**, 1794 (1988).